Article

Supramolecular p–n-Heterojunctions by Co-Self-Organization of Oligo(*p*-phenylene Vinylene) and Perylene Bisimide Dyes

Frank Wrthner, Zhijian Chen, Freek J. M. Hoeben, Peter Osswald, Chang-Cheng You, Pascal Jonkheijm, Jeroen v. Herrikhuyzen, Albertus P. H. J. Schenning, Paul P. A. M. van der Schoot, E. W. Meijer, Edwin H. A. Beckers, Stefan C. J. Meskers, and Ren A. J. Janssen

J. Am. Chem. Soc., **2004**, 126 (34), 10611-10618• DOI: 10.1021/ja0475353 • Publication Date (Web): 07 August 2004

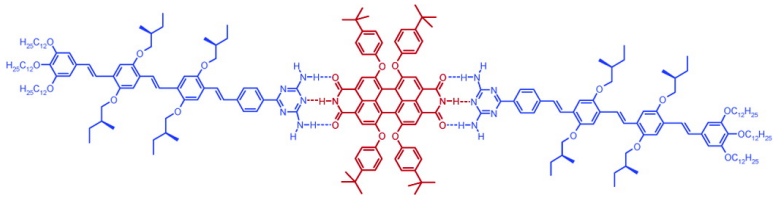

More About This Article

J|A|C|S
ARTICLES
Published on Web 08/07/2004

Supramolecular p−n-Heterojunctions by Co-Self-Organization of Oligo(*p*-phenylene Vinylene) and Perylene Bisimide Dyes

Frank Würthner,*,† Zhijian Chen,† Freek J. M. Hoeben,‡ Peter Osswald,† Chang-Cheng You,† Pascal Jonkheijm,‡ Jeroen v. Herrikhuyzen,‡ Albertus P. H. J. Schenning,*,‡ Paul P. A. M. van der Schoot,§ E. W. Meijer,‡ Edwin H. A. Beckers,‡ Stefan C. J. Meskers,‡ and René A. J. Janssen‡

Contribution from the Institut für Organische Chemie, Universität Würzburg, Am Hubland, D-97074 Würzburg, Germany, Laboratory of Macromolecular and Organic Chemistry, Eindhoven University of Technology, P.O. Box 513, 5600 MB Eindhoven, The Netherlands, and Department of Applied Physics, Eindhoven University of Technology, P.O. Box 513, 5600 MB Eindhoven, The Netherlands

Received April 28, 2004; E-mail: wuerthner@chemie.uni-wuerzburg.de; A.P.H.J.Schenning@tue.nl

Abstract: Comparative studies on hydrogen-bonded versus covalently linked donor−acceptor−donor dye arrays obtained from oligo(*p*-phenylene vinylene)s (OPVs) as donor and bay-substituted perylene bisimides (PERYs) as acceptor dyes are presented. Both systems form well-ordered *J*-type aggregates in methylcyclohexane, but only hydrogen-bonded arrays afford hierarchically assembled chiral OPV−PERY dye superstructures consisting of left-handed helical $\pi-\pi$ co-aggregates (CD spectroscopy) of the two dyes that further assemble into right-handed nanometer-scale supercoils in the solid state (AFM study). In the case of hydrogen-bonded arrays, the stability of the aggregates in solution increases with increasing conjugation length of the OPV unit. The well-defined co-aggregated dyes presented here exhibit photoinduced electron transfer on subpicosecond time scale, and thus, these supramolecular entities might serve as valuable nanoscopic functional units.

Introduction

Dye aggregates have received considerable attention from academic as well as industrial points of view. Thus, *J*-type cyanine dye aggregates that had been discovered independently by Jelley and Scheibe already in the 1930s[1] became the most applied photosensitizers in silver halide photography,[2] and triphenylene,[3] porphyrin,[4] and phthalocyanine[5] dye aggregates have been investigated as photoconductors[6] for electrophotography. Recently, new applications of dye aggregates have been proposed in the fields of highly sensitive biosensors,[7] field-effect transistors,[8] and solar cells.[9] However, for solar cells it is necessary to have two different charge carrier systems that are of n- and of p-type as well as absorbance features that closely match the solar spectrum. In the past, these complex features have been accomplished by mesoporous n-type TiO_2 coated with a photosensitizer dye and a p-type conducting electrolyte ("Grätzel" cell)[10] or by a p-type conducting polymer that was loaded with large amounts of n-type conductive fullerene derivates.[11] Recently, Friend and Müllen have introduced an alternative to conducting polymers and applied a liquid-crystalline hexabenzocoronene as the p-type semiconductor and a perylene bisimide dye as n-type material.[12a] From all these examples, it is evident that the formation of a photosensitive p−n-junction is the central unit of an organic solar cell but has been mastered mainly on the meso- and macroscopic scale thus far.[11,12]

In the given article we now report, to our knowledge, the first example of a co-assembled p−n-junction that incorporates

† Universität Würzburg.
‡ Laboratory of Macromolecular and Organic Chemistry, Eindhoven University of Technology.
§ Department of Applied Physics, Eindhoven University of Technology.

(1) (a) Scheibe, G. *Angew. Chem.* **1936**, *49*, 563. (b) Scheibe, G. *Angew. Chem.* **1937**, *50*, 212−219. (c) Jelley, E. *Nature* **1936**, *138*, 1009−1010.
(2) (a) Wolthaus, L.; Schaper, A.; Möbius, D. *Chem. Phys. Lett.* **1994**, *225*, 322−326. (b) Koti, A. S. R.; Periasamy, N. *J. Mater. Chem.* **2002**, *12*, 2313−2317 and references therein.
(3) Adam, D.; Schuhmacher, P.; Simmerer, J.; Häussling, L.; Siemensmeyer, K.; Etzbach, K.-H.; Ringsdorf, H.; Haarer, D. *Nature* **1994**, *371*, 141−143.
(4) Schenning, A. P. H. J.; Benneker, F. B. G.; Geurts, H. P. M.; Liu, X. Y.; Nolte, R. J. M. *J. Am. Chem. Soc.* **1996**, *118*, 8549−8552.
(5) (a) van Nostrum, C. F.; Picken, S. J.; Schouten, A.-J.; Nolte, R. J. M. *J. Am. Chem. Soc.* **1995**, *117*, 9957−9965. (b) Engelkamp, H.; Middelbeek, S.; Nolte, R. J. M. *Science* **1999**, *284*, 785−788.
(6) Law, K.-Y. *Chem. Rev.* **1993**, *93*, 449−486.
(7) (a) Chen, L.; McBranch, D. W.; Wang, H.-L.; Helgeson, R.; Wudl, F.; Whitten, D. G. *Proc. Natl. Acad. Sci. U.S.A.* **1999**, *96*, 12287−12292. (b) Jones, R. M.; Lu, L.; Helgeson, R.; Bergstedt, T. S.; McBranch, D. W.; Whitten, D. G. *Proc. Natl. Acad. Sci. U.S.A.* **2001**, *98*, 14769−14772.
(8) (a) Würthner, F. *Angew. Chem., Int. Ed.* **2001**, *40*, 1037−1039. (b) Kraft, A. *ChemPhysChem* **2001**, *2*, 163−165.
(9) Wöhrle, D.; Meissner, D. *Adv. Mater.* **1991**, *3*, 129−138.
(10) Hagfeld, A.; Grätzel, M. *Acc. Chem. Res.* **2000**, *33*, 269−277.
(11) (a) Nelson, J. *Curr. Opin. Solid State Mater. Sci.* **2002**, *6*, 87−95. (b) Brabec, C. J.; Winder, C.; Sariciftci, N. S.; Hummelen, J. C.; Dhanabalan, A.; van Hal, P. A.; Janssen, R. A. J. *Adv. Funct. Mater.* **2002**, *12*, 709−712.
(12) (a) Schmidt-Mende, L.; Fechtenkötter, A.; Müllen, K.; Moons, E.; Friend, R. H.; MacKenzie, J. D. *Science* **2001**, *293*, 1119−1122. For other works on organic solar cell that apply perylene bisimide dyes, see: (b) Tang, C. W. *Appl. Phys. Lett.* **1986**, *48*, 183−185. (c) Breeze, A. J.; Salomon, A.; Ginley, D. S.; Gregg, B. A.; Tillmann, H.; Hörhold, H.-H. *Appl. Phys. Lett.* **2002**, *81*, 3085−3087. (d) Park, L. Y.; Hamilton, D. G.; McGehee, E. A.; McMenimen, K. A. *J. Am. Chem. Soc.* **2003**, *125*, 10586−10590.

p-type oligo(*p*-phenylene vinylene) (OPV) derivatives and n-type perylene bisimide (PERY) derivatives on a nanoscopic scale,[13] a progress that has become possible by combining our earlier activities on hydrogen-bond-directed aggregation processes of pure OPVs[14] and pure PERY dyes.[15] When the mobility of the p- and n-type charge carriers is sufficiently large, they could migrate within the individual stacks, leading to a p−n-heterojunction on the nanoscale. Such heterojunctions could provide an efficient photoactive unit for organic solar cells.[12] These highly defined nanostructures can serve as excellent model systems for the better understanding of solid-state device properties. Moreover, donor−acceptor assemblies are important not only for solar cells but also for addressing fundamental questions in biological electron-transfer processes in which hydrogen bonding plays a crucial role.[16]

Experimental Section

General Methods. The synthetic procedures for compounds **1a**,[14c] **1b**,[14b] **1c**,[14c] **2**,[15b] **3**,[17b] **4**[15c], and **5**[18] have been published previously. The solvents for spectroscopic studies were of spectroscopic grade and used as received. UV/vis spectra were measured on a spectrometer equipped with a temperature controlling system. The steady state fluorescence spectra were measured on a standard spectrofluorometer. The fluorescence quantum yields in methylcyclohexane (MCH) were determined by the optically dilute method using *N*,*N*′-di(2,6-diisopropylphenyl)-1,6,7,12-tetraphenoxyperylene-3,4:9,10-tetracarboxylic acid bisimide as reference ($\Phi_f = 0.96$ in chloroform).[19] The CD spectra were recorded on a commercial spectropolarimeter with temperature controller.

Formation of the Complex. The complexes were prepared by dissolving a 2:1 ratio of OPV to perylene bisimide in MCH and using sonication treatment (5 min) and heating.

Aggregation Studies in MCH by UV/Vis Spectroscopy. The UV/vis spectra of the **1**−**2**−**1** and **5**−**2**−**5** complexes and compound **3** were recorded at different concentrations and different temperatures in MCH. The apparent molar extinction coefficients at several wavelengths were fitted by nonlinear least-squares regression analysis to the isodesmic (or equal *K*) model.[15c,20] The binding constant was obtained by fitting the change of the apparent molar extinction coefficient of the aggregated perylene bisimide.

AFM Measurements. Atomic force microscopy (AFM) measurements were carried out at room temperature with an AFM equipped with a Nanoscope IIIa controller in the Tapping Mode regime. Glass substrates were cleaned intensively by rinsing with acetone and ethanol followed by drying under a nitrogen flow. Polyethylenedioxythiophene: polystyrenesulfonate (PEDOT:PSS) (in water) was spin-coated at room temperature as follows: After filtering the complete solution over a black rim FP 30/5.0 CN filter unit, the complete surface of the substrate was covered. Then, the following spin rates were applied on a spin-coater: 500 rpm for 7 s followed by 1500 rpm for 35 s. Finally, the substrate was placed on a hot plate (100 °C) for 1 min to remove excessive water. On top of the PEDOT layer, complex **1b**−**2**−**1b** (10 g/L MCH) was spin-coated at room temperature as follows: After the substrate was placed on the chuck, the surface of the substrate was covered with solution, followed by spinning the samples at spin rates of 500 rpm for 7 s, followed by 1500 rpm for 35 s.

Microfabricated silicon cantilever tips with a resonance frequency of approximately 330 kHz and a spring constant of about 42 Nm^{-1} were used. The scan rate varied from 0.5 to 1.5 Hz. The set-point amplitude ratio ($r_{sp} = A_{sp}/A_0$, where A_{sp} is the amplitude setpoint and A_0 is the amplitude of free oscillation) was adjusted to 0.9. All AFM images shown here were subjected to a first-order plane-fitting procedure to compensate for sample tilt. AFM analysis was done offline.

Transient Femtosecond Photoinduced Absorption Spectroscopy. The femtosecond laser system used for pump−probe experiments consisted of an amplified Ti/sapphire laser. The single pulses from a cw mode-locked Ti/sapphire laser were amplified by a Nd:YLF laser using chirped pulse amplification, providing 150-fs pulses at 800 nm with an energy of 750 μJ and a repetition rate of 1 kHz. The pump pulses at 455 nm were created via optical parametric amplification (OPA) of the 800-nm pulse by a BBO crystal into infrared pulses, which were then 2 times frequency doubled via BBO crystals. The probe beam was generated in a separate optical parametric amplification setup in which the 1450-nm pulses were created, and an RG 850-nm cutoff filter was used to avoid contributions of residual probe light (800 nm) from the OPA. The pump beam was focused to a spot size of about 1 mm^2 with an excitation flux of 1 mJ cm^{-2} per pulse. The probe beam was reduced in intensity compared to the pump beam by using neutral density filters. The pump beam was linearly polarized at the magic angle of 54.7° with respect to the probe, to cancel out orientation effects in the measured dynamics. The temporal evolution of the differential transmission was recorded using an InGaAs detector by a standard lock-in technique at 500 Hz.

Photovoltaic Devices. The devices were fabricated and characterized as described before.[14b]

Results and Discussion

Preparation of Hydrogen-Bonded and Covalent Donor−Acceptor−Donor Arrays. The hydrogen-bonded donor−acceptor−donor complexes **1**−**2**−**1** (Chart 1) were obtained through the complementary hydrogen bonding between the diaminotriazine groups and imide groups in MCH.[15b] Covalent compounds **3**[17] and **4**[15c] have been included in this study for comparison, as well as the supramolecular complex **5**−**2**−**5** (Chart 1).[18]

UV/Vis and Fluorescence Properties of the Hydrogen-Bonded and Covalently Bonded OPV−PERY−OPV Systems. To determine the stoichiometry of the **1**−**2**−**1** complexes, UV/vis titration experiments in MCH were carried out. In all cases, a pronounced bathochromic shift from $\lambda_{max} \approx 560$ nm to $\lambda_{max} \approx 600$ nm for the PERY absorption maximum of the S_0−S_1 electronic transition was observed upon adding aliquots of diaminotriazine derivatives **1a**, **1b**, **1c**, or **5**, respectively, to PERY **2**. If the concentration of **1b** was kept constant and **2**

(13) A short communication of this work has been published: Schenning, A. P. H. J.; van Herrikhuyzen, J.; Jonkheijm, P.; Chen, Z.; Würthner, F.; Meijer, E. W. *J. Am. Chem. Soc.* **2002**, *124*, 10252−10253.
(14) (a) Schenning, A. P. H. J.; Jonkheijm, P.; Peeters, E.; Meijer, E. W. *J. Am. Chem. Soc.* **2001**, *123*, 409−416. (b) El-ghayoury, A.; Schenning, A. P. H. J.; van Hal, P. A.; van Duren, J. K. J.; Janssen, R. A. J.; Meijer, E. W. *Angew. Chem., Int. Ed.* **2001**, *40*, 3660−3663. (c) Jonkheijm, P.; Hoeben, F. J. M.; Kleppinger, R.; van Herrikhuyzen, J.; Schenning, A. P. H. J.; Meijer, E. W. *J. Am. Chem. Soc.* **2003**, *125*, 15941−15949. (d) Jonkheijm, P.; Miura, A.; Zdanowska, M.; Hoeben, F. J. M.; de Feyter, S.; Schenning, A. P. H. J.; de Schryver, F.; Meijer, E. W. *Angew. Chem., Int. Ed.* **2004**, *43*, 74−78.
(15) (a) Würthner, F.; Thalacker, C.; Sautter, A. *Adv. Mater.* **1999**, *11*, 754−758. (b) Würthner, F.; Thalacker, C.; Sautter, A.; Schärtl, W.; Ibach, W.; Hollricher, O. *Chem.−Eur. J.* **2000**, *6*, 3871−3885. (c) Würthner, F.; Thalacker, C.; Diele, S.; Tschierske, C. *Chem.−Eur. J.* **2001**, *7*, 2245−2253. (d) Thalacker, C.; Würthner, F. *Adv. Funct. Mater.* **2002**, *12*, 209−218. (e) Sautter, A.; Thalacker, C.; Heise, B.; Würthner, F. *Proc. Natl. Acad. Sci. U.S.A.* **2002**, *99*, 4993−4996. (f) Würthner, F. *Chem. Commun.* **2004**, 1564−1579.
(16) Piotrowiak, P. *Chem. Soc. Rev.* **1999**, *28*, 143−150.
(17) (a) Miura, A.; Chen, Z.; Uji-i, H.; De Feyter, S.; Zdanowska, M.; Jonkheijm, P.; Schenning, A. P. H. J.; Meijer, E. W.; Würthner, F.; de Schryver, F. *J. Am. Chem. Soc.* **2003**, *125*, 14968−14969. (b) Beckers, E. H. A.; Meskers, S. C. J.; Schenning, A. P. H. J.; Chen, Z.; Würthner, F.; Janssen, R. A. J. *J. Phys. Chem. A*, published online Aug 3, 2004. http://dx.doi.org/10.1021/jp048980n.
(18) Hirschberg, J. H. K. K.; Ramzi, A.; Sijbesma, R. P.; Meijer, E. W. *Macromolecules* **2003**, *36*, 1429−1432.
(19) Gvishi, R.; Reisfeld, R.; Burshtein, Z. *Chem. Phys. Lett.* **1993**, *213*, 338−344.
(20) (a) Martin, R. B. *Chem. Rev.* **1996**, *96*, 3043−3064. (b) Baxter, N. J.; Williamson, M. P.; Lilley, T. H.; Haslan, E. *J. Chem. Soc., Faraday Trans. 2* **1996**, *92*, 231−234.

Chart 1. Chemical Structures of the Compounds Used in This Study

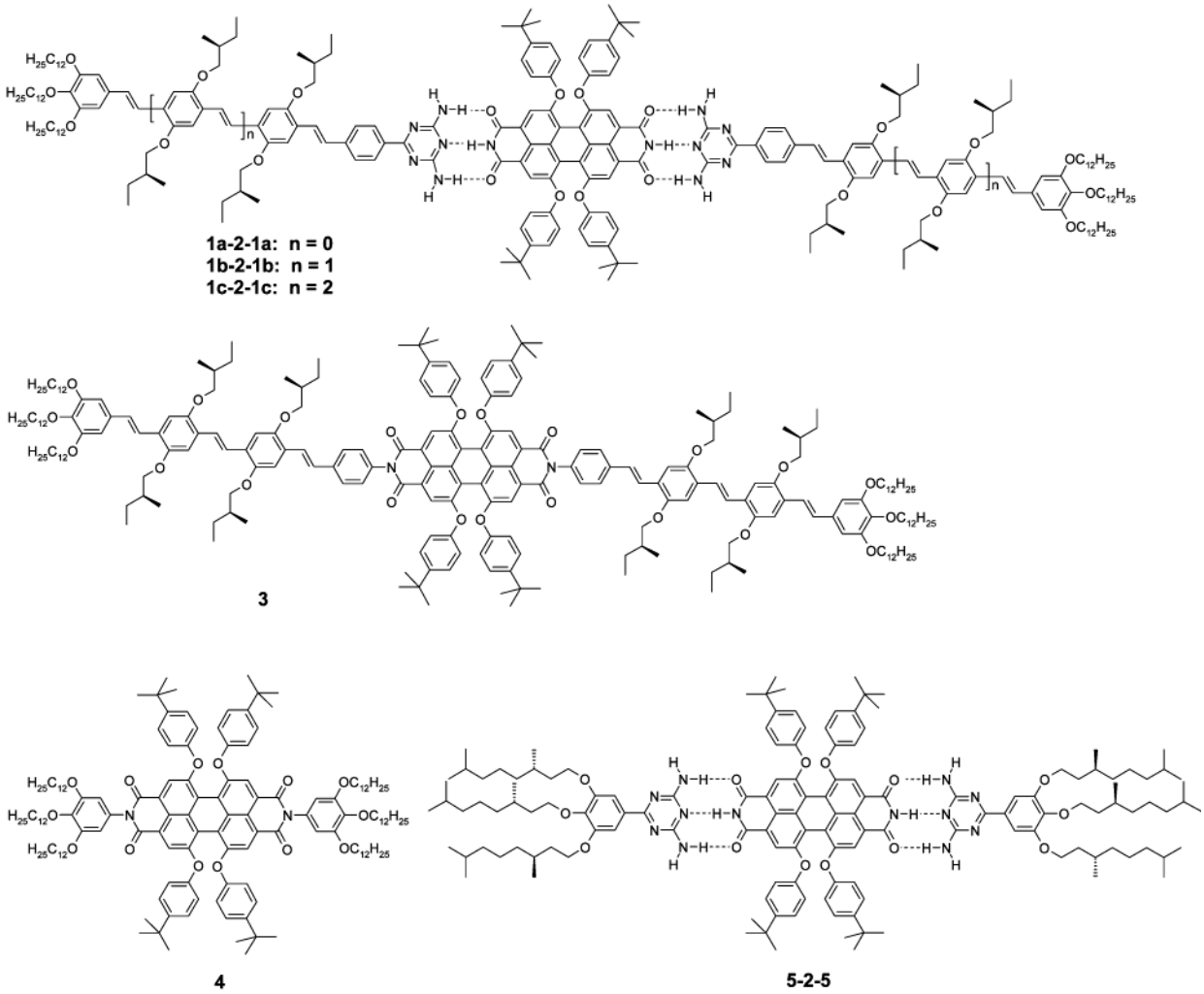

was added in portions, a bathochromic shift was observed for the OPV absorption maximum from $\lambda_{max} = 436$ nm to $\lambda_{max} = 450$ nm (Figure S1 in Supporting Information). Analysis of the titration curve shows the formation of 2:1 hydrogen-bonded complexes of the individual compounds in accordance with the hydrogen-bonding pattern shown in Chart 1.

For compound **3**, UV/vis spectra were recorded in CH_2Cl_2 at a concentration where no aggregation takes place ($c = 4 \times 10^{-7}$ mol L^{-1}).[17a] An intense absorption band was observed at $\lambda_{max} = 436$ nm that is attributed to the OPV unit.[21] PERY-related transitions are located at $\lambda_{max} = 581$ nm with a vibronic shoulder at 541 nm.[15,19] The transitions corresponding to the PERY and OPV moieties can be easily distinguished and interpreted as a simple sum of the spectra of the two components. In the less-polar solvent MCH at low concentration ($c = 4 \times 10^{-7}$ mol L^{-1}), the absorption maxima were shifted 13 nm hypsochromically because of a solvatochromic effect ($\lambda_{max} = 429$ nm and $\lambda_{max} = 568$ nm).[22] At higher concentrations stacking occurs, which leads to a red shift of the absorption maxima indicating *J*-type aggregates (vide infra).

Compounds **1a**, **1b**, and **1c** have fluorescence quantum yields in $CHCl_3$ of 0.81, 0.67, and 0.50, respectively. PERY **2** is highly fluorescent in CH_2Cl_2 with a quantum yield of 0.98.[15b] In CH_2Cl_2 or $CHCl_3$ at concentrations $<10^{-5}$ mol L^{-1}, **1**−**2**−**1** complexes disassemble into their building blocks and the strong fluorescence of both compounds is maintained.[23] However, when the **1**−**2**−**1** complexes are formed in MCH, the fluorescence of both dyes is drastically quenched and the optimal quenching of fluorescence was obtained when all imide binding sites of **2** are hydrogen-bonded to **1** (Figure 1, only the titration experiment of **1b** is shown).

Typically, dye aggregates whose absorption maxima are shifted to longer wavelength (*J*-aggregates) show intense fluorescence but here the fluorescence of both dyes was drastically quenched. On the basis of the redox potentials of the given chromophores or their analogues,[15c,17b] this observation is rationalized by a photoinduced electron (and energy) transfer process (PET) from the OPV donor to the PERY acceptor chromophore. A Stern−Volmer constant of 6.5×10^5 L mol^{-1} was calculated from the Stern−Volmer plot. For compound **3**, likewise strong fluorescence quenching of PERY dyes was observed by the attachment of the electron-donating OPV moieties. As a result, the fluorescence of **3** is not detectable in

(21) Peeters, E.; van Hal, P. A.; Meskers, S. C. J.; Janssen, R. A. J.; Meijer, E. W. *Chem.*−*Eur. J.* **2002**, *8*, 4470−4474.
(22) Reichardt, C. *Chem. Rev.* **1994**, *94*, 2319−2358.
(23) Molecularly dissolved species will be present, since the binding constant for hydrogen bonding in these solvents is very low. A binding constant of 243 M^{-1} in $CDCl_3$ was determined for **1b** and a related diimide acceptor, e.g., *N*-(2,5-di-*tert*-butylphenyl)-1,8-dicarboxy-*N*′-hydrogen-4,5-dicarboxy-naphthalenediimide.

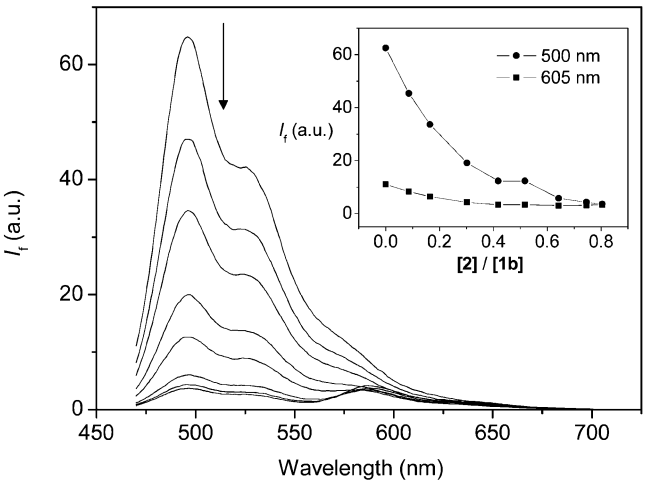

Figure 1. Fluorescence titration experiments performed in MCH. Concentration of **1b** = 3.7×10^{-6} mol L^{-1}, concentration of **2** ranges from 0 to 3×10^{-6} mol L^{-1}. The arrow indicates changes upon addition of **2**. Excitation wavelength = 450 nm. (Inset) The changes of the fluorescence intensity at 500 and 605 nm are plotted as a function of [**2**]/[**1b**].

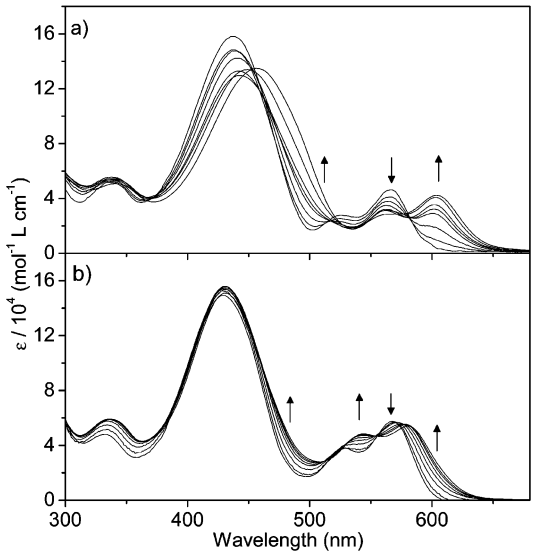

Figure 2. UV/vis absorption spectra in MCH at room temperature of **1b**−**2**−**1b** (a) (concentration from 1.0×10^{-7} mol L^{-1} to 5.0×10^{-5} mol L^{-1}) and **3** (b) (concentration from 1.0×10^{-7} mol L^{-1} to 1.0×10^{-4} mol L^{-1}). Arrows indicate changes upon increasing concentration.

CH_2Cl_2 (Φ_f < 0.001), again suggesting a very efficient photoinduced electron transfer (PET) between the electron donor OPV and the electron acceptor PERY. However, in the less polar solvent MCH, compound **3** shows a fluorescence band that is characteristic for a tetra-*tert*-butylphenoxy-substituted PERY, but the fluorescence quantum yield is only 0.06 (Figure S2 in Supporting Information). The fact that this value is independent of the excitation wavelength and that the fluorescence excitation spectrum of **3** monitored at 593 nm closely matches the absorption spectrum suggest a nearly quantitative energy transfer from the two OPV units to the PERY core followed by fluorescence from the PERY S_1 state in competition with the PET process. Apparently the electron-transfer rate is slower in the apolar solvent MCH than in CH_2Cl_2, a result which can be explained by Marcus theory.[17b]

Aggregation Studies by UV/Vis and CD Spectroscopy. Since both OPV and PERY compounds form dye aggregates in aliphatic solvents, as revealed by our previous studies,[14,15] $\pi-\pi$ aggregation was also expected for the current two-component systems. For both covalently bonded and hydrogen-bonded systems, UV/vis absorption spectra show pronounced changes of the optical properties upon concentration variation (Figure 2, Table S1 in Supporting Information). For complexes **1**−**2**−**1** and **5**−**2**−**5**, a new bathochromically shifted band around 600 nm appears for the PERY S_0-S_1 electronic transition with increasing concentration (Figure 2a, only the spectra of **1b**−**2**−**1b** are shown). The changes in λ_{max} are much larger than those for all PERY aggregates studied thus far[15] and suggest the formation of *J*-type aggregates.[24] The observed bathochromic shift is apparently not due to the charge-transfer interactions because the absorption bands of both OPV (donor) and PERY (acceptor) are bathochromically shifted at higher concentrations (Table S1 in Supporting Information). According to the exciton coupling theory, the magnitude of bathochromic shift is related to the stacking distance of the $\pi-\pi$ aggregated dyes, the angle between the stack axis and the transition dipole moment

Table 1. Aggregation Constants *K* and Corresponding Gibbs Free Binding Energies ($\Delta G°$) of **1**−**2**−**1**, **3**, **4**, and **5**−**2**−**5** in MCH at Room Temperature

	K/L mol^{-1}	$-\Delta G°$/kJ mol^{-1}
1a−**2**−**1a**	3.8×10^5	31.3
1b−**2**−**1b**	1.5×10^6	35.2
1c−**2**−**1c**	1.1×10^7	39.5
3	1.3×10^6	34.9
4	1.2×10^5	29.0
5−**2**−**5**	4.1×10^4	26.3

("slipping angle") as well as rotational displacement of the dyes in a helical aggregate (see CD studies).[24,25] In all three hydrogen-bonded complexes, bathochromic shifts between 36 and 49 nm were observed for the perylene bisimide S_0-S_1 band, corresponding to a lowering of the energy level of the first excited state by about 1100−1400 cm^{-1}. Such pronounced spectral displacement suggests that the distance between the chromophores is rather short and/or that the angle between the stack axis and the transition dipole moment is significantly smaller than 54.7°.[24,25] At the same time, a red shift of about 20 nm was observed for the OPV absorption band for all three hydrogen-bonded OPV systems. For the covalent compound **3** (Figure 2b), less pronounced spectral changes were observed with bathochromic shifts of only 12 nm for the PERY band and no shift for the OPV band, suggesting that the angle between the stack axis and the transition dipole moment is closer to the magic angle, with respect to the **1**−**2**−**1** complexes.[25]

The aggregation constants for **1**−**2**−**1** and **3** (Table 1, Figure 3) were calculated by fitting the spectroscopic data from the UV/vis dilution studies to the isodesmic (or equal *K*) model[20] by nonlinear least-squares regression analysis. In this model, equal $\pi-\pi$ binding constants for both faces are assumed, leading to a one-dimensional aggregate.[15c,20] In contrast to simple covalent compounds such as **3** and **4**, a more complicated situation is given for the **1**−**2**−**1** and **5**−**2**−**5** complexes because hydrogen bonding interactions are also present. On a logarithmic

(24) (a) Czikkely, V.; Försterling, H. D.; Kuhn, H. *Chem. Phys. Lett.* **1970**, *6*, 11−14; 207−210. (b) Bohn, P. W. *Annu. Rev. Phys. Chem.* **1993**, *44*, 37−60. (c) *J-Aggregates*; Kobayashi, T., Ed.; World Scientific: Singapore, 1996.

(25) Kasha, M.; Rawls, H. R.; El-Bayoumi, M. A. *Pure. Appl. Chem.* **1965**, *11*, 371−392.

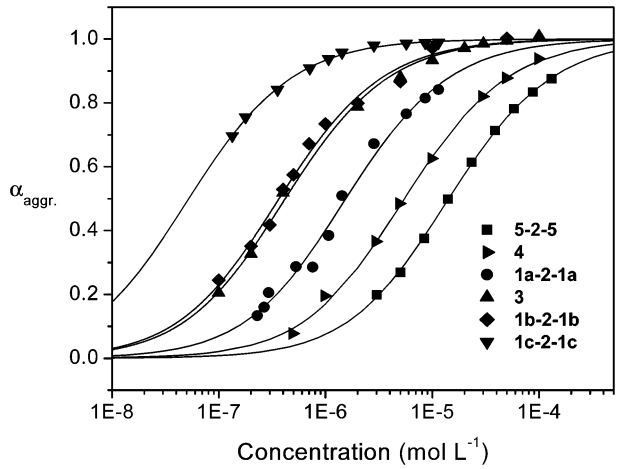

Figure 3. Fraction of aggregated component α_{aggr} as a function of the concentration of **1**−**2**−**1**, **3**, **4**, and **5**−**2**−**5** in MCH at room temperature. The curves were calculated by fitting the ratio of the absorption of aggregated and nonaggregated PERY to the isodesmic (or equal *K*) model.

scale, Figure 3 compares the calculated isotherms for the stacking of the **1**−**2**−**1** and **5**−**2**−**5** hydrogen-bonded complexes, covalently bonded OPV−PERY compound **3,** and the reference compound **4** at room temperature. In addition, Table 1 provides the calculated aggregation constants and Gibbs free binding energies. According to this study, the strength of $\pi-\pi$ stacking increases almost linearly with the conjugation length of the PERY-attached OPVs. Successive elongation of OPV units, increasing the effective $\pi-\pi$ overlap between neighboring molecules in the stack, repeatedly increases the binding constants by 1 order of magnitude. Note that the free energy of dimerization of thiacyanine dyes increases steadily with increasing conjugation length.[26] A remarkable observation, however, is that **1b**−**2**−**1b** and **3** exhibit almost identical binding constants despite the fact that hydrogen-bonded and covalent systems are compared, suggesting that $\pi-\pi$ interactions are the main driving force for the formation of stacks.[27]

In the temperature-dependent UV/vis spectroscopic studies, similar spectral changes were observed as in the concentration-dependent studies for all three hydrogen-bonded complexes **1**−**2**−**1** (Figure 4a, only the spectral changes for **1b**−**2**−**1b** are shown) and covalently bonded compound **3** (Figure 4b). At temperatures higher than 70 °C in MCH, the absorption spectra were similar to those of the molecularly dissolved compounds in chloroform at room temperature.

Coinciding with the changes in the UV/vis spectra, strong CD signals (vide infra) for the OPV and PERY bands decreased at temperatures higher than 40 °C and were completely lost at 60 °C (Figure S3 in Supporting Information), while an increase of the photoluminescence of **2** at $\lambda = 591$ nm ($\lambda_{ex} = 575$ nm) was observed upon disassembly at elevated temperature. Upon cooling, a similar absorption spectrum was obtained as that before heating, indicating full reversibility. From Figure 5, "melting" temperatures are calculated for the phase transitions

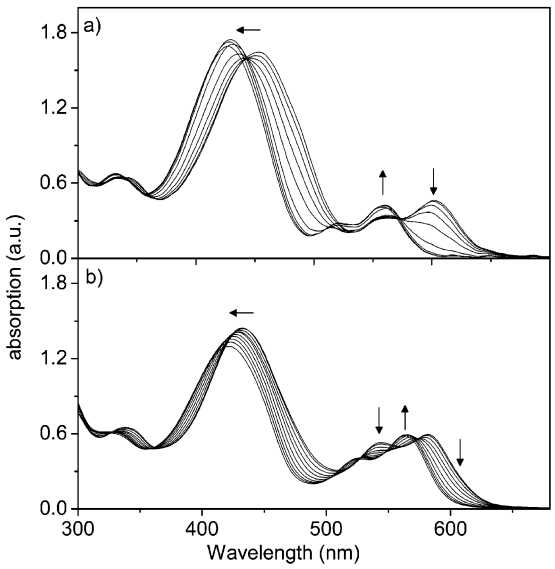

Figure 4. Temperature-dependent UV/vis spectra from 10 to 80 °C of **1b**−**2**−**1b** (a) and **3** (b) in MCH at concentration of 1×10^{-5} mol L^{-1}. Arrows indicate changes with increasing temperature.

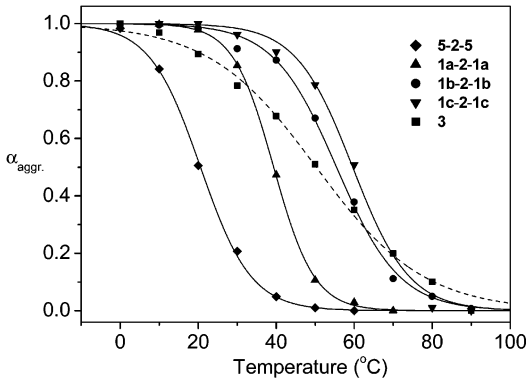

Figure 5. Aggregate fraction α_{aggr} versus temperature of the complexes **1**−**2**−**1**, **5**−**2**−**5**, and **3** in MCH according to UV/vis spectroscopy. Concentration in all cases 1×10^{-5} mol L^{-1}.

from aggregated dyes to molecularly dissolved species. In agreement with the concentration-dependent measurements, there is a clear dependence of the aggregate melting transition on OPV conjugation length. On elongation of the π-conjugated backbone, the melting transition increases from $T_m = 21$ °C (**5**−**2**−**5**) to 39 °C (**1a**−**2**−**1a**), 55 °C (**1b**−**2**−**1b**), and 60 °C (**1c**−**2**−**1c**). The melting of the stacks takes place in a very narrow temperature range, and the observed trend is similar to that found earlier for the aggregates of ureidotriazine OPVs.[14d] As a reference, the melting transition of **3** is also plotted ($T_m =$ 51 °C), which shows a more gradual transition suggesting different entropy and enthalpy effects in those systems (vide infra). Apparently, the formation of dye co-aggregates highly benefits from the hydrogen bonding, ensuring a more planar system as compared to the covalently linked one. The increase in melting transition seems to level off, which is in full agreement with our results recently obtained on columnar aggregates of hydrogen-bonded OPVs.[14d]

The enthalpy and entropy contributions to the Gibbs free energy changes for the self-assembly process of **3** and **1b**−**2**−**1b** complex were evaluated from a Van't Hoff plot (Figure 6) according to the equation $-RT \ln(K/K_0) = \Delta H° - T\Delta S°$, where $K_0 = 1$ L mol^{-1}. From concentration-dependent UV/vis experi-

(26) West, W.; Pearce, S. *J. Phys. Chem.* **1965**, *69*, 1894−1903.
(27) However, the aggregation strength of **4** is higher than that of **5**−**2**−**5**, which might be explained in terms of the different aliphatic chains of the trialkoxybenzene wedges used. For $\pi-\pi$ interactions of water soluble derivatives of parent perylene bisimide, see: (a) Wang, W.; Han, J. J.; Wang, L.-Q.; Li, L.-S.; Shaw, W. J.; Li, A. D. Q. *Nano Lett.* **2003**, *3*, 455−458. (b) Wang, W.; Li, L.-S.; Helms, G.; Zhou, H.-H.; Li, A. D. Q. *J. Am. Chem. Soc.* **2003**, *125*, 1120−1121. (c) Wang, W.; Wan, W.; Zhou, H.-H.; Niu, S.; Li, A. D. Q. *J. Am. Chem. Soc.* **2003**, *125*, 5248−5249.

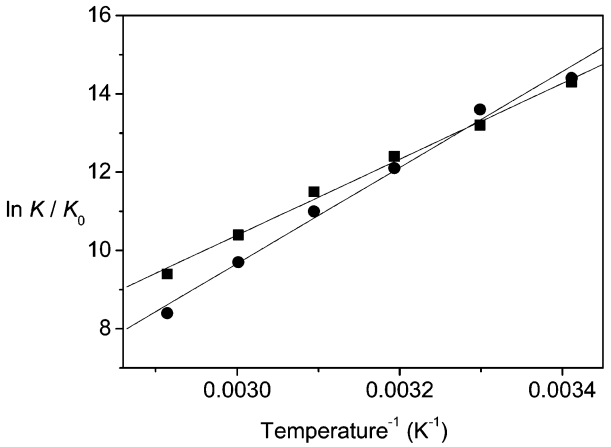

Figure 6. Van't Hoff plot for the temperature dependence of the aggregation constant K of **1b**−**2**−**1b** complex (●) and **3** (■) in MCH. The K values were obtained from concentration-dependent UV/vis spectra and $K_0 = 1$ L mol^{-1}.

ments at different temperatures, the binding constants K were determined by nonlinear regression analysis (Table S2 in Supporting Information). For **3**, a plot of ln K versus T^{-1} shows a perfect linear relationship (correlation coefficient $r = 0.997$), and the standard enthalpy and entropy were determined to be $\Delta H° = -81 \pm 3$ kJ mol^{-1} and $\Delta S° = -155 \pm 10$ J mol^{-1} K^{-1}. For the **1b**−**2**−**1b** complex, the linear regression analysis afforded a correlation coefficient $r = 0.995$ with values of $\Delta H° = -102 \pm 5$ kJ mol^{-1} and $\Delta S° = -226 \pm 16$ J mol^{-1} K^{-1}. The negative enthalpy and negative entropy values indicate that for both systems self-assembly is enthalpy-driven. The large enthalpy changes originate obviously from the effective stacking of the π-systems, which, however, simultaneously reduces the intramolecular mobility to cause negative entropy changes. The significantly more negative enthalpy changes found for the hydrogen-bonded triad **1b**−**2**−**1b** is in agreement with the steeper slope of the melting curve in comparison with **3** (vide supra). The slope is directly related to the enthalpy change of the melting of the stacks.[28] The larger negative entropy change observed for the **1b**−**2**−**1b** complex is reasonable since the self-assembly of **1b**−**2**−**1b** aggregates involves more components than in the case of **3**.

The pronounced bathochromic shift for the **1**−**2**−**1** complex with respect to **3**[15] gives evidence of a stronger excitonic coupling.[25] It is reasonable to relate this difference to the coplanarity of the diaminotriazine units of OPV with the PERY imide groups because of the triple hydrogen-bonding complex that could facilitate a tighter packing of the PERY π-systems (comparable to the base stacking in DNA).[27] In contrast, for the covalently bonded OPV−PERY compound **3**, the phenyl groups at the imide's N positions prefer to be twisted to the imide planes according to molecular modeling studies and crystal structures on related compounds.[29]

Because of the presence of chiral side chains at the OPV units and the inherent axial chirality of bay-substituted PERY dyes (racemic, with a low-energy barrier for interconversion in solution)[30] CD measurements were carried out for **1**−**2**−**1** and **5**−**2**−**5** complexes and compound **3** in MCH (Figure 7). Surprisingly, for **1a**−**2**−**1a** no and for **3** only a very weak Cotton effect was observed, while for **1b**−**2**−**1b** and **1c**−**2**−**1c** complexes strong bisignated signals were observed for the S_0-S_1 transitions of the OPV units **1b** and **1c** with a zero crossing at 456 and 459 nm, respectively. In the same concentration range, a negative CD signal of the PERY chromophores arose at 600 nm for **1b**−**2**−**1b**, **1c**−**2**−**1c**, and **5**−**2**−**5** complexes. The bisignated CD signals for OPV moieties are indicative for chiral excitonic couplings that arise if the chromophores are aggregated in close proximity with their transition dipoles oriented in a helical fashion.[15d,31] The signal change from positive to negative with increasing λ indicates a left-handed helical arrangement of the transition dipoles, which are polarized along the long axis of the OPVs.[32] On the other hand, for the S_0-S_1 transition of the PERY chromophores, only a negative signal can be observed at 600 nm. This CD effect cannot be ascribed to a chiral excitonic coupling as no obvious bisignated band could be observed. It is, therefore, likely that this signal arises from the axial chirality originating from the nonplanar structure of bay-substituted PERY **2**.[15d] For this family of compounds, the *P* and *M* enantiomers could be directly observed as racemate in the crystalline state where close contacts between the molecules of opposite chirality are preferred.[29,30] In the nonaggregated state in dilute solution, the same amounts of *P* and *M* enantiomers are present and $P \rightleftarrows M$ interconversion is rapid on the NMR time scale. Upon aggregation, this interconversion is slowed and enrichment of one enantiomer is possible under the influence of the chiral OPV aggregates because of the formation of diastereomeric complexes. Here, the negative CD signal of the PERY band can be related to the preferential formation of *M* enantiomers caused by the left-handed helical stacking of the **1**−**2**−**1** complex.[33] Figure 8 shows a model for such aggregates that is based on our optical data and molecular modeling. However, it has to be noted that

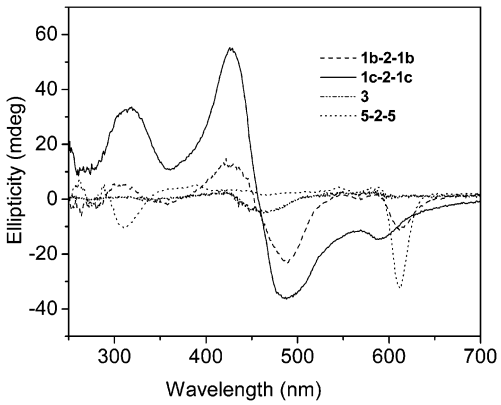

Figure 7. CD spectra of **1b**−**2**−**1b**, **1c**−**2**−**1c**, and **5**−**2**−**5** at concentration of 4×10^{-5} mol L^{-1} and **3** at concentration of 1×10^{-4} mol L^{-1} in MCH at 20 °C.

(28) van der Schoot, P.; Michels, M. A J.; Brunsveld, L.; Sijbesma, R. P.; Ramzi, A. *Langmuir* **2000**, *16*, 10076−10083.
(29) The crystal structure of a tetrachloro-substituted perylene bisimide with 4-dodecylphenyl substituents at imide N atoms shows an average torsion angle of 79° between the plane of the phenyl groups and the imide units: Chen, Z.; Debije, M. G.; Debaerdemaeker, T.; Osswald, P.; Würthner, F. *ChemPhysChem* **2004**, *5*, 137−140.
(30) Würthner, F.; Sautter, A.; Schilling, J. *J. Org. Chem.* **2002**, *67*, 3037−3044.
(31) Langeveld-Voss, B. M. W.; Beljonne, D.; Shuai, Z.; Janssen, R. A. J.; Meskers, S. C. J.; Meijer, E. W.; Brédas, J.-L. *Adv. Mater.* **1998**, *10*, 1343−1348.
(32) Harada, N.; Nakanishi, K. *Circular Dichroism Spectroscopy*; Oxford University Press: Oxford, 1983.
(33) Stacking model studies show that owing to the steric effect of the bay-substituents, for *M* enantiomers a left-handed and for *P* enantiomers a right-handed helical stacking is preferred.

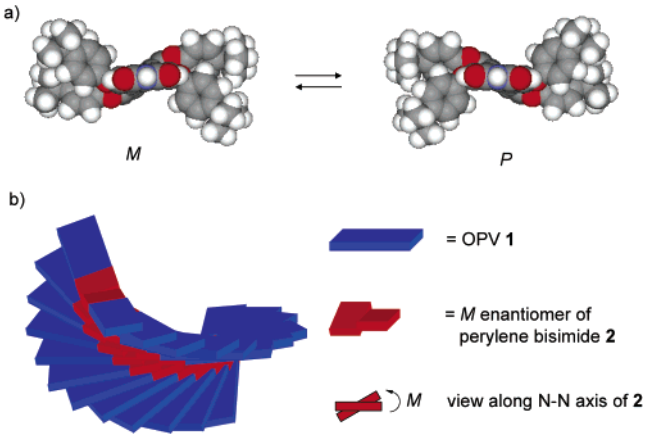

Figure 8. (a) Energy-minimized (CAChe 5.0 MM2 force field) structures of the *M* (left) and the *P* (right) enantiomers of perylene bisimide **2**. (b) Left-handed helical stacking model for the **1b**−**2**−**1b** complex from OPV **1b** and *M* enantiomer of perylene bisimide **2**.

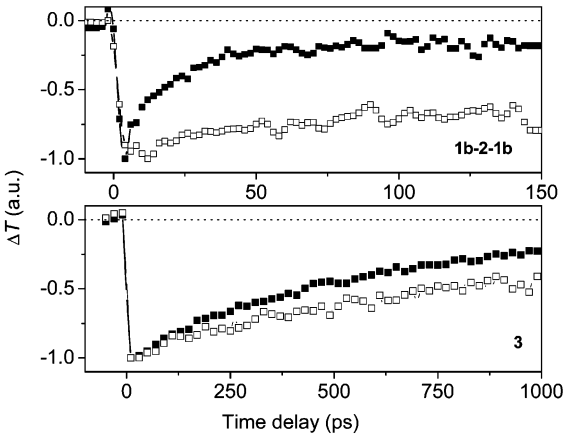

Figure 9. Differential transmission dynamics of **1b**−**2**−**1b** (top) and **3** (bottom) at 20 °C (■) and 80 °C (□) recorded at 1450 nm (low-energy absorption of OPV radical cations) after excitation at 455 nm. Both samples are 5×10^{-5} mol L^{-1} in MCH.

our data do not allow us to determine to which extent the $P \rightleftarrows M$ equilibrium for the PERY chromophore is shifted under the influence of the chiral OPVs. On the basis of Figure 7, the most pronounced induction of chirality for the perylene bisimide subunit is observed for **5**−**2**−**5** followed by **1b**−**2**−**1b** and **1c**−**2**−**1c**. On the other hand, for compound **3**, only very weak CD signals are given for the OPV band and no signal for the PERY band was observed. Therefore, we can conclude that chiral side chains at the OPV units are not sufficient to transfer chirality to the PERY unit in **1a**−**2**−**1a** and **3**. Instead, only upon helical stacking of the OPV units does the chirality transfer to the co-aggregated PERY units takes place, leading to well-defined dye aggregates (see also AFM studies vide infra).

Photoinduced Electron Transfer in Aggregated and Non-aggregated States. Previously performed bias-dependent scanning tunneling microscopy (STM) and electrochemical measurements for **3** suggest that the fluorescence quenching observed for three OPV−PERY systems can be explained by a photoinduced electron-transfer process from the OPV to the PERY moieties.[17a] Femtosecond pump−pulse spectroscopic measurements were performed in MCH to determine the rate for charge separation in the triad systems that have the same OPV moieties (**1b**−**2**−**1b** and **3**). When excited at 455 nm, where mainly OPV absorbs, the low-energy absorption of the OPV radical cation at 1450 nm can be detected, indicating that photoinduced electron transfer takes place.[17b] The rates for charge separation (k_{CS}) and recombination (k_{CR}) were determined by monitoring the temporal evolution of the absorption at 1450 nm (Figure 9). For both investigated systems, **1b**−**2**−**1b** and **3**, the rise of the signal occurred within 1 ps, indicative of a very efficient and fast charge formation ($k_{CS} > 10^{12}$ s^{-1}). Charge recombination was much slower and varied at room temperature from $k_{CR} = 6.3 \times 10^{10}$ s^{-1} (corresponding to a time constant of 16 ps) for **1b**−**2**−**1b** to $k_{CR} = 2.0 \times 10^{9}$ s^{-1} (time constant of 500 ps) for **3**. Under the experimental conditions (5×10^{-5} mol L^{-1} in MCH), both compounds are aggregated. Hence, it is impossible to determine whether the charges are formed within a covalently or hydrogen-bonded **1**−**2**−**1** (supra)molecular triad unit or if OPV and PERY molecules from neighboring triad units within the stack are involved. Because of the longer distance between redox centers in the hydrogen-bonded system, one would expect that the rate of intramolecular charge transfer within the triad **1b**−**2**−**1b** should be lower or comparable to **3**. Accordingly, the fact that a much higher recombination rate was observed for **1b**−**2**−**1b** is indicative that electron transfer in the co-aggregated assemblies occurs between the donor and acceptor molecules that belong to different triads. This conclusion is in accordance with the CD and UV/vis data and the structural model in Figure 8. Thus, because of the more coplanar arrangement of the OPV and PERY units in the hydrogen-bonded assemblies, the donor and acceptor dyes are packed more tightly. This leads to shorter distances between OPV and PERY units of neighboring triads compared to the distance within a triad.

An attempt was made to establish the effect of aggregation on the charge recombination rate by studying molecularly dissolved compounds obtained at higher temperature in the same apolar environment. At 80 °C, only a small difference in the rate for charge recombination was observed for compound **3**. This suggests that the electron-transfer processes are localized to the molecular OPV−PERY−OPV triad irrespective of the further assembly of these molecules. On the other hand, in the **1b**−**2**−**1b** complex, the temperature effect is more pronounced. The time constant for charge recombination increases from 16 ps at 20 °C to more than 200 ps at 80 °C. The reduced rate for charge recombination must be related to disassembled species of **1b**−**2**−**1b** hydrogen-bonded units or even dissociated compounds present at higher temperature. The distance between the redox centers in these complexes is much longer than that in the $\pi-\pi$ aggregate assembly (close contact between OPV and PERY of neighboring triads), and therefore, the rate for charge recombination will also decrease.

Solid-State Properties. The **1b**−**2**−**1b** assemblies were also investigated on glass covered with a conducting layer of PEDOT:PSS, a device relevant support (vide infra). AFM revealed helical fibers lying on top of a structureless, amorphous matrix of **1b**−**2**−**1b** (Figure 10A). The width of the smallest fiber that can be resolved is about 4 nm (Figure 10B, upper arrow). Molecular modeling studies suggest that the long axis of the **1b**−**2**−**1b** complex is about 7 nm in size and the short axis about 1 nm. Also, thicker and right-handed helical rodlike fibers were observed with a length of several micrometers and a width of about 13 nm (Figure 10B, bottom arrow, the distance has been corrected for tip dimensions).[34] It is assumed that

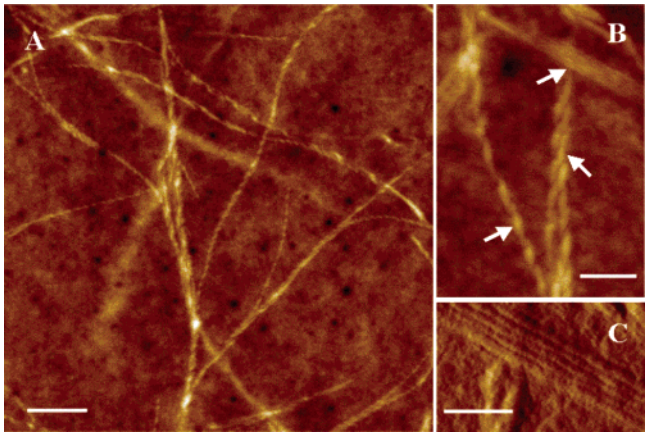

Figure 10. (A) Tapping mode AFM topographic images of the **1b**−**2**−**1b** complex after spin-coating from MCH (scale bar 500 nm) on a glass// PEDOT:PSS slide. (B) Locally enlarged picture (scale bar 100 nm). (C) Enlarged picture of the location around the upper arrow (scale bar 50 nm).

multiple small fibers are coiled into each other to afford those thicker supercoils that minimize the van der Waals interactions between the smallest fibers. An additional feature that could be observed is a further self-assembly to double-helical or even larger intertwined assemblies (Figure 10B, middle arrow). The composition of the bulk of this film itself remains elusive, since AFM only probes the surface characteristics. Nevertheless, these studies show that the transfer of chiral information in **1b**−**2**−**1b** aggregates takes place over several hierarchical levels. First, the chiral information of the side chain is transferred to the OPV−OPV stacks and simultaneously to the hydrogen-bonded PERY, leading to left-handed helical stacking of the OPV and axial chirality of the PERY, as demonstrated by the CD results (Figure 7). Finally, those left-handed fibers intertwine to give right-handed supercoils (Figure 10). Such change of handedness is not surprising and has already been observed for aggregates of chiral phthalocyanines, where the chromophores aggregated into right-handed fibers first and then assembled further into left-handed supercoils.[5b]

Recently, Friend et al. have reported a photovoltaic device made from a mixture of a p-type discotic liquid crystalline hexabenzocoronene and a n-type perylene bisimide dye, in which a phase segregation on micrometer-scale takes place.[12a] With the present hydrogen-bonded OPV−PERY−OPV complexes, fibers containing p-type and n-type molecules can be prepared on a much smaller scale (1−20 nm). These nanoscopic aggregates may provide higher charge transport efficiency than the reported mesoscopic systems if an appropriate orientation of the former aggregates can be achieved. Accordingly, a photovoltaic device (glass/ITO/PEDOT:PSS/**1b**−**2**−**1b**/LiF:Al) was constructed by spin-coating a 100-nm thick layer of the **1b**−**2**−**1b** complex from MCH on a PEDOT:PSS-coated ITO substrate. Preliminary experiments revealed poor diode behavior with an open circuit voltage of 0.74 V and a low current density (2.6 μA cm^{-2}). As shown in our AFM study, the co-aggregated dyes tend to organize themselves laterally on the surface, which is not favorable for the charge transport to the metal electrodes. A more favorable orientation of the aggregates, i.e., perpendicular to the surface, may well provide more efficient solar cells that we hope to realize in the future on the basis of these or similarly constructed supramolecular p−n-heterojunctions.

(34) Samori, P.; Franke, V.; Mangel, T.; Müllen, K.; Rabe, J. *Opt. Mater.* **1998**, *9*, 390−394.

Conclusion

This work showed that supramolecular p−n-heterojunctions can be formed by a hierarchical co-self-organization of OPV donor and PERY acceptor chromophores. Supramolecular OPV−PERY−OPV units are initially formed via hydrogen bonding and subsequently self-assemble into chiral stacks by $\pi-\pi$ interactions. There is a distinct dependence of aggregate stability on OPV conjugation length, which is apparent from concentration and temperature-dependent optical measurements. On the basis of transient absorption spectroscopy, fluorescence quenching of OPV and PERY in the assembly can be related to photoinduced electron transfer that takes place even in apolar aliphatic solvents. Because the packing of the donor and acceptor dyes in these stacks is dependent on the individual components and their mode of connection (hydrogen-bonded or covalent), different CD effects and electron recombination rates are observed. Such well-defined co-aggregated dyes may serve as valuable nanoscopic functional building blocks for solid-state devices, which are often hampered by the intrinsic disorder as a result of the preparation method.

Acknowledgment. We are grateful to the Deutsche Forschungsgemeinschaft (DFG) for financial support (Grant Wu 317/5). Part of this research has been supported by the Netherlands Organization for Scientific Research (CW-NWO) through a grant in the PIONIER program. The research of S.C.J.M. has been made possible by a fellowship of the Royal Dutch Academy of Arts and Sciences. We would like to acknowledge Marc Koetse and Herman F. M. Schoo (TNO Industrial Technology/Polymer Technology, The Netherlands) for the construction of the solar cells.

Supporting Information Available: UV/vis absorption data of complexes **1**−**2**−**1**, **5**−**2**−**5**, and compound **3** (Table S1); aggregation constant of **1b**−**2**−**1b** and **3** in MCH at different temperature (Table S2); UV/vis titration experiment of **1b** with **2** (Figure S1); UV/vis, fluorescence emission, and excitation spectra of **3** (Figure S2); and temperature-dependent CD spectra of **1b**−**2**−**1b** complex (Figure S3). This material is available free of charge via the Internet at http://pubs.acs.org.

JA0475353